Acta Crystallographica Section D
**Biological Crystallography**
ISSN 0907-4449

# Monoclinic guanidinoacetate methyltransferase and gadolinium ion-binding characteristics

**Junichi Komoto,[a] Yoshimi Takata,[a,b] Taro Yamada,[a] Kiyoshi Konishi,[b]† Hirofumi Ogawa,[b] Tomoharu Gomi,[b]‡ Motoji Fujioka[b] and Fusao Takusagawa[a]***

[a]Department of Molecular Biosciences, University of Kansas, 1200 Sunnyside Avenue, Lawrence, KS 66045-7534, USA, and [b]Department of Biochemistry, Toyama Medical and Pharmaceutical University, Faculty of Medicine, Sugitani, Toyama 930-01, Japan

† Present address: Department of Microbiology, The Nippon Dental University, 1-9-20 Fujimi, Chiyoda-ku, Tokyo 102, Japan.
‡ Present address: Scientific Instrument Center, Toyama Medical and Pharmaceutical University, Sugitani, Toyama 930-0194, Japan.

Correspondence e-mail: xraymain@ku.edu



Received 13 April 2003
Accepted 30 June 2003

**PDB References:** guanidinoacetate methyltransferase, 1p1b, r1p1bsf; Gd derivative, 1p1c, r1p1csf.

Guanidinoacetate methyltransferase (GAMT) is the enzyme that catalyzes the last step of creatine biosynthesis. The enzyme is found in abundance in the livers of all vertebrates. Recombinant rat liver GAMT truncated at amino acid 37 from the N-terminus has been crystallized with *S*-adenosylhomocysteine (SAH) in a monoclinic modification and the crystal structure has been determined at 2.8 Å resolution. There are two dimers in the crystallographic asymmetric unit. Each dimer has non-crystallographic twofold symmetry and is related to the other dimer by pseudo-$4_3$ symmetry along the crystallographic *b* axis. The overall structure of GAMT crystallized in the monoclinic modification is quite similar to the structure observed in the tetragonal modification [Komoto *et al.* (2002), *J. Mol. Biol.* **320**, 223–235], with the exception of the loop containing Tyr136. In the monoclinic modification, the loops in three of the four subunits have a catalytically unfavorable conformation and the loop of the fourth subunit has a catalytically favorable conformation as observed in the crystals of the tetragonal modification. From the structures in the monoclinic and tetragonal modifications, we can explain why the Y136F mutant enzyme retains considerable catalytic activity while the Y136V mutant enzyme loses the catalytic activity. The crystal structure of a Gd derivative of the tetragonal modification has also been determined. By comparing the Gd-derivative structure with the native structures in the tetragonal and the monoclinic modifications, useful characteristic features of Gd-ion binding for application in protein crystallography have been observed. Gd ions can bind to proteins without changing the native protein structures and Gd atoms produce strong anomalous dispersion signals from Cu $K\alpha$ radiation; however, Gd-ion binding to protein requires a relatively specific geometry.

## 1. Introduction

Guanidinoacetate methyltransferase (*S*-adenosyl-L-methionine:guanidinoacetate *N*-methyltransferase; GAMT; EC 2.1.1.2), first found in pig liver by Cantoni & Vignos (1954), is the enzyme that catalyzes the last step of creatine biosynthesis. The enzyme is found in abundance in the livers of all vertebrates.

The GAMT catalytic reaction (Fig. 1) is a sequential ordered bi-bi reaction with SAM as the first substrate (Takata *et al.*, 1994). In humans, the biosynthesis of creatine is reported to represent about 75% of the total utilization of methionine through *S*-adenosylmethionine (SAM; Mudd & Poole, 1975) and thus GAMT is believed to be the major enzyme involved in the metabolic conversion of SAM to *S*-adenosylhomocysteine (SAH) in vertebrates (Mudd *et al.*, 1980). A

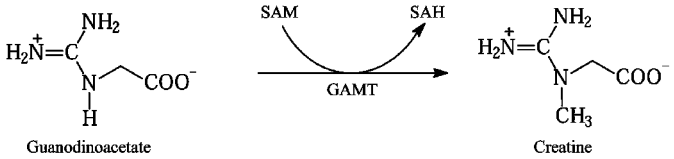


**Figure 1**
GAMT catalytic reaction.

hereditary disease with extrapyramidal motor disorder and extremely low concentrations of creatine in the brain, serum and urine has been described (Stöckler *et al.*, 1994) and shown to arise from a deficiency of GAMT in the liver (Stöckler *et al.*, 1996, 1997).

The rat enzyme expressed in *Escherichia coli* tends to be cleaved of 36 amino-acid residues at the N-terminus during purification. The truncated enzyme has been crystallized in two modifications (monoclinic and tetragonal; Komoto *et al.*, 1999). The structure of tetragonal modification has been determined at 2.5 Å resolution (Komoto *et al.*, 2002). The truncated enzyme forms a dimer and each subunit has a ternary complex structure. In the active site of each subunit, a SAH molecule binds at the first substrate (SAM) binding site and Arg220 of the partner subunit of the dimer binds at the second substrate (guanidinoacetate; GAA) binding site. Thus, the dimer structure represents not only a ternary complex of GAMT, but also that of a protein arginine methyltransferase. It is noted that the truncated enzyme does not catalyze creatine formation from SAM and GAA.

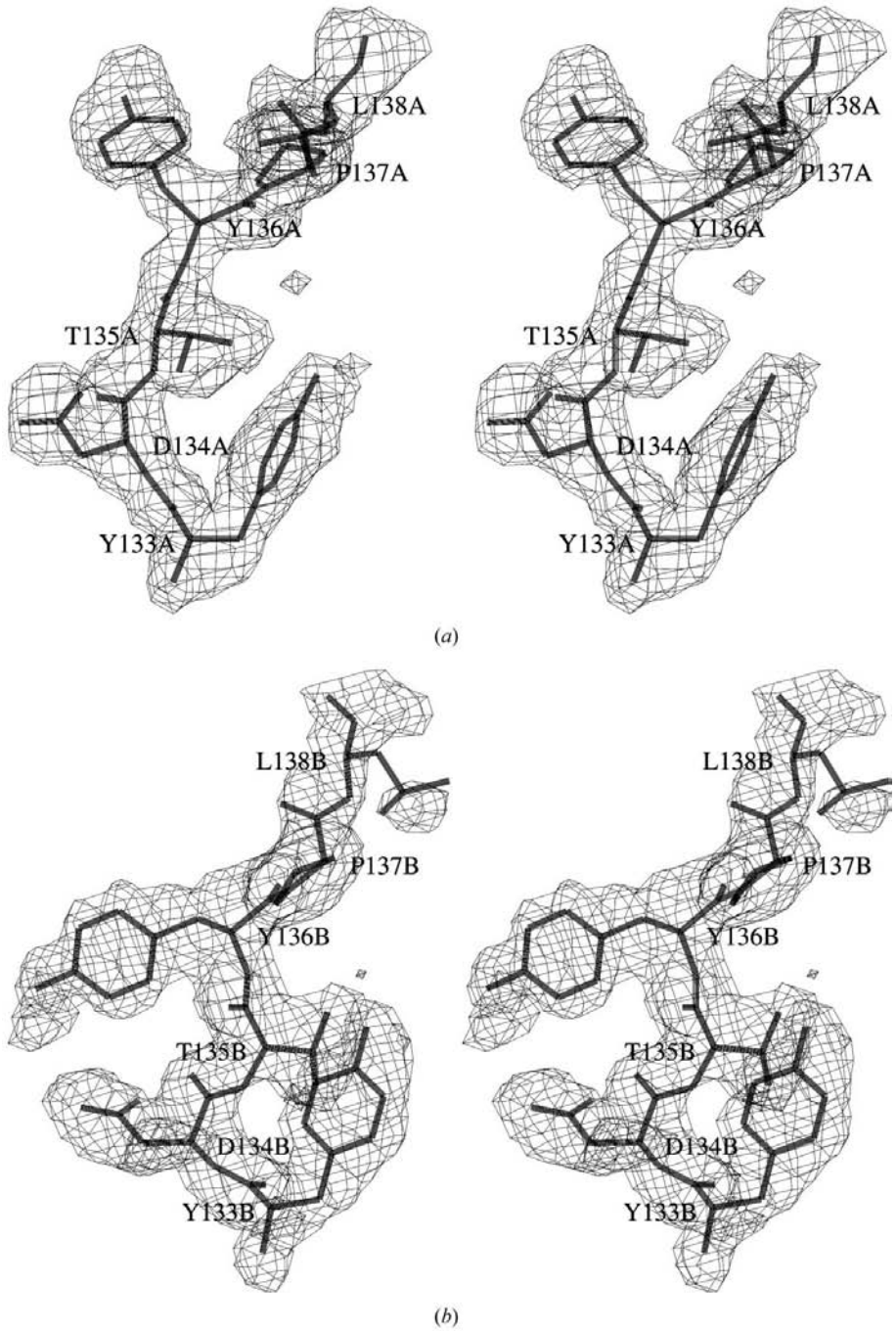


**Figure 2**
($2F_o - F_c$) maps showing electron-density peaks from residues 133–138 of subunits *A* and *B*. The map orientations are similar to those in Fig. 3. The contours are drawn at the 1.0$\sigma$ level. Figs. 2 and 5 were produced using a locally developed program.

Catalytic mechanisms for GAMT and protein arginine methyltransferase have been proposed on the basis of the dimer structure (Komoto *et al.*, 2002). Limited proteolysis (Fujioka *et al.*, 1991), chemical modification studies (Takata & Fujioka, 1992) and site-directed mutagenesis studies on Asp134 (Takata *et al.*, 1994) are consistent with the proposed catalytic mechanism of GAMT. Tyr136 is located near the bound SAH, but the Y136F mutation indicates that Tyr136 is not involved in the catalytic mechanism (Takata *et al.*, 1994). However, the Y136V mutant enzyme loses its activity (Hamahata *et al.*, 1996). These mutation data could not be explained by the GAMT structure crystallized in a tetragonal modification.

Although the preparation of proteins containing SeMet residues is the current major direction for protein phasing, the classic MIR method with heavy-atom soaking is still popular. The structure of GAMT (tetragonal modification) was initially determined by a single isomorphous replacement

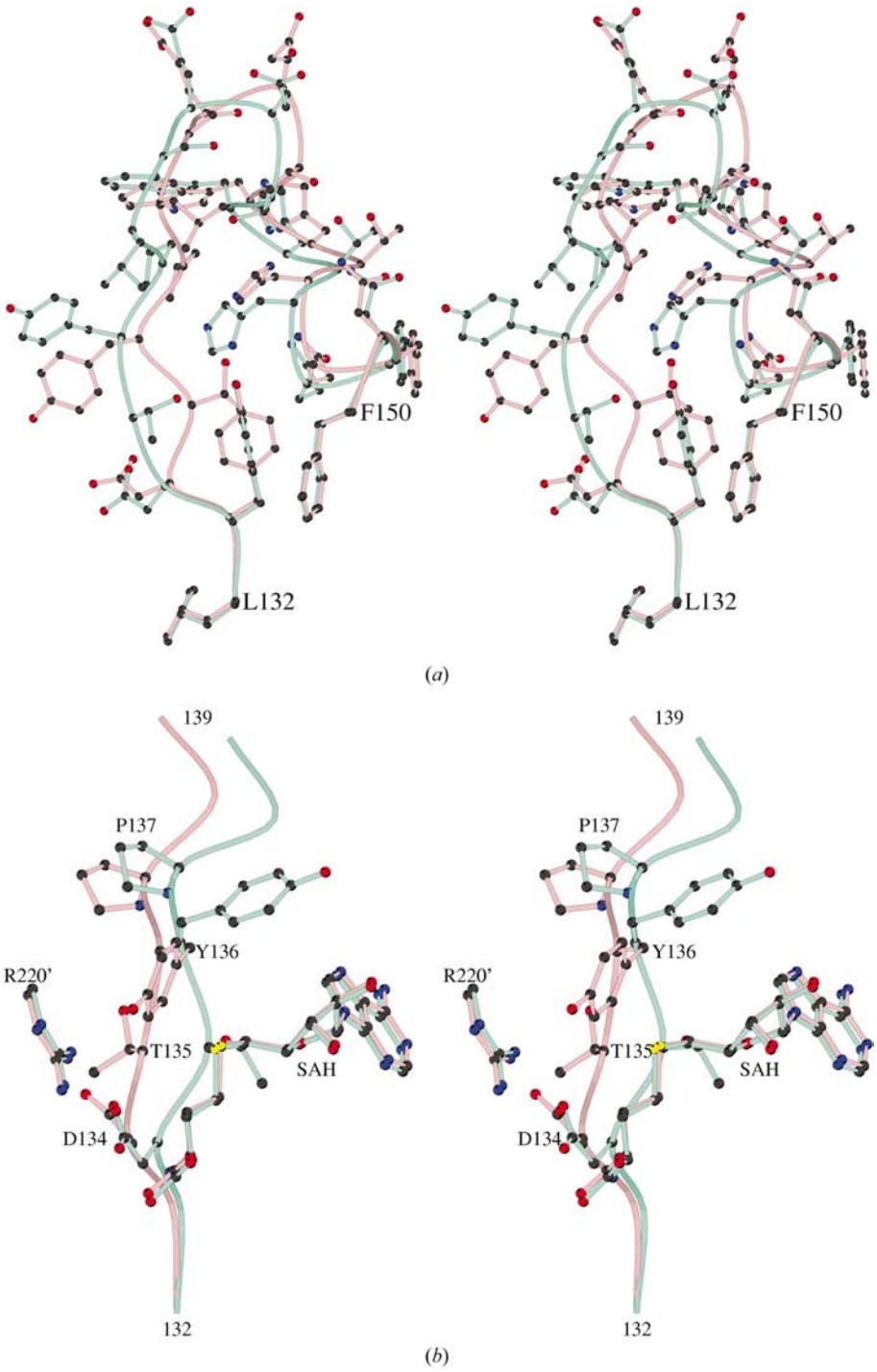


**Figure 3**
(*a*) Superimposed view of two polypeptides from residues 132–150 of subunits *A* and *B*. The polypeptides that belong to subunit *A* and *B* are illustrated in aquamarine and light pink, respectively. (*b*) Superimposed view of two polypeptides from residues 134–137 of subunits *A* and *B* with the bound SAH and Arg220′ of the partner subunit. The same color codes are applied. Figs. 3, 4 and 5 were produced using *MOLSCRIPT* (Kraulis, 1991).

with anomalous scattering (SIRAS) method using a Gd-derivative crystal. In the structure determination, the Gd ion displayed two characteristics: (i) the Gd ion only binds in one site of the dimer GAMT and (ii) Gd ion does not bind to GAMT in the monoclinic crystals.

Here, we report the crystal structure of GAMT crystallized in a monoclinic modification. With this structure and the structure in the tetragonal modification, we can explain why the Y136V mutated enzyme loses its catalytic activity while the Y136F mutant enzyme retains its catalytic activity, why the GAMT dimer in the tetragonal modification contains only one Gd ion per dimer and why Gd ion does not bind to GAMT in the monoclinic crystals.

## 2. Materials and methods

### 2.1. Purification and crystallization procedures

The GAMT used in this study was recombinant rat enzyme produced in *E. coli* JM109 transformed with a pUCGAT9-1 plasmid that contains the coding sequence of rat GAMT cDNA (Ogawa *et al.*, 1988). The enzyme was purified to homogeneity from *E. coli* extracts by gel filtration over Sephacryl S-200 and DEAE-cellulose chromatography as described previously (Komoto *et al.*, 1999).

The hanging-drop vapour-diffusion method was employed for crystallization of the enzyme. Crystals were grown from a solution containing 50 m*M* MES buffer pH 6.5, 1 m*M* dithiothreitol, 2 m*M* SAH, 1 m*M* GAA, 8%(*w*/*v*) PEG 8000 with a protein concentration of 10 mg ml$^{-1}$ in a 277 K cold room. Needle-shaped crystals suitable for X-ray diffraction studies (~0.70 × 0.15 × 0.15 mm) were grown in one week. Careful observation indicated there to be two differently shaped crystals in the same drops. X-ray diffraction experiments indicated that the enzyme crystallized in two different modifications (monoclinic with space group $P2_1$ and tetragonal with space group $P4_3$).

### 2.2. Data measurement

The crystals of the monoclinic modification from a hanging drop were scooped up in a nylon loop and dipped into a cryoprotectant solution containing 50 m*M* MES buffer pH 6.5, 1 m*M* dithiothreitol, 8%(*w*/*v*) PEG 8000 and 20%(*v*/*v*) ethylene glycol for 10 s before being cryocooled in liquid nitrogen. The cryocooled crystals were

transferred to a Rigaku R-AXIS IIc imaging-plate X-ray diffractometer with a rotating-anode X-ray generator as an X-ray source (Cu $K\alpha$ radiation, operated at 50 kV and 100 mA). The X-ray beam was focused to 0.3 mm by confocal optics (Osmic Inc., USA). The diffraction data were measured to 2.8 Å resolution at 93 K. The data were processed with the programs *DENZO* and *SCALEPACK* (Otwinowski & Minor, 1997). The data statistics are given in Table 1.

The tetragonal gadolinium-derivative crystals were prepared by the soaking method: native crystals of the tetragonal modification were incubated in an artificial mother liquor containing 50 m*M* MES buffer pH 6.5, 1 m*M* DTT, 8%(*w*/*v*) PEG 8000, 30%(*v*/*v*) ethylene glycol and 1 m*M* $GdCl_3$ for 10 min before being cryocooled in liquid nitrogen. The diffraction data were measured to 2.5 Å resolution at 93 K and were processed by the same method used for the data collected from the monoclinic crystal.

### 2.3. Structure determination of the monoclinic modification

The unit-cell parameters and space group indicate that the asymmetric unit contains four subunits. The crystal structure was determined by a molecular-replacement procedure using the program *AMoRe* (Navaza, 1994). A subunit of the tetragonal modification was used as the search model. ($F_o - F_c$) maps showed no significant electron-density peaks for amino-acid residues 1–43, suggesting that the crystallized enzyme was truncated at amino-acid residue 37, as observed in the structure of tetragonal modification; this was confirmed by a mass spectrum (Komoto *et al.*, 2002). ($F_o - F_c$) maps showed a significant residual electron-density peak in the region of the active site. Since GAMT was crystallized in the presence of an excess of SAH (2 m*M*), an SAH molecule was fitted into the difference electron-density peak. The model was refined with the positional protocol and then the simulated-annealing procedure of *X-PLOR* (Brünger, 1993). Initially, the four subunits were tightly restrained to have the same structure. However, ($2F_o - F_c$) maps showed irregular electron-density peaks around residues 130–150 in subunit *A*. Therefore, residues 130–150 in subunit *A* were excluded from the non-crystallographic symmetry restraints. Refinement of isotropic temperature factors for individual atoms was carried out using the individual *B*-factor refinement procedure of *X-PLOR* with bond and angle restraints. During the final refinement stage, well defined residual electron-density peaks in difference maps were assigned to water molecules if the peaks were at hydrogen-bonding distance from the protein molecules. The final crystallographic *R* factor was 0.215 for observed data ($3\sigma$ cutoff) in the resolution range 8.0–2.8 Å. $R_{\rm free}$ for a randomly selected 10% of the data is 0.288.

The structure of the Gd derivative was refined using the coordinates of the tetragonal modification as the initial model. The structure was refined with the same procedures as were applied to the monoclinic structure. No non-crystallographic symmetry restraints were applied. The final crystallographic *R* factor was 0.194 for observed data ($3\sigma$ cutoff) in the resolution range 8.0–2.5 Å resolutio. $R_{\rm free}$ for a randomly selected 10% of the data is 0.288.

## 3. Results and discussion

The crystallographic refinement parameters (Table 1), final ($2F_o - F_c$) maps (Fig. 2) and conformational analysis by *PROCHECK* (Laskowski *et al.*, 1993) indicate that the crystal structure of GAMT crystallized in the monoclinic modification has been determined successfully. The crystallographic asymmetric unit contains two dimers (*AB* and *CD*) and each subunit in a dimer is related to the other subunit by a non-crystallographic twofold axis. The crystal structure has a pseudo-$4_3$ axis along the crystallographic *b* axis and dimer *AB* is related to dimer *CD* by this pseudo-$4_3$ symmetry. Therefore, the molecular packing in the monoclinic modification is quite similar to that observed in the tetragonal modification (Komoto *et al.*, 2002). The structures of subunits *B*, *C* and *D* are very similar to each other and the r.m.s.d. between them is less than 0.054 Å. Subunit *A* is significantly different from the other subunits (the r.m.s.d. is 0.74 Å). For simplicity, the following description mainly refers to subunits *A* and *B*.

The overall structure of each subunit is quite similar to that observed in the tetragonal modification. The 37 residues at the N-terminus are truncated and residues 38–42 are disordered. Each subunit is composed of a single domain, with the peptide chain organized into seven $\alpha$-helices and seven $\beta$-strands. The polypeptide is folded into a typical $\alpha/\beta$ open sandwich structure. The topology is –$\alpha$1(45–56)–$\beta$1(61–66)–$\alpha$2(77–72)–$\beta$2(82–89)–$\alpha$3(92–102)–$\beta$3(108–113)–$\alpha$4(116–119)–$\beta$4(128–133)–$\alpha$5(146–158)–$\beta$5(159–167)–$\alpha$6(170–176)–$\alpha$7(184–199)–$\beta$6(206–212)–$\beta$7(226–233)–.

The structure of subunit *A* is quite similar to that found in the tetragonal modification. The major differences between subunit *A* and *B* are seen between amino-acid residues 133 and 146 (Fig. 3*a*). The r.m.s.d. between subunits *A* and *B* is reduced from 0.74 to 0.29 Å when residues 133–146 are excluded from the least-squares fitting calculation, indicating that the loop between $\beta$4 and $\alpha$5 has two different conformations (conformation *A* for the loop in subunit *A* and conformation *B* for the loop in subunit *B*). As shown in Fig. 3(*b*), a notable difference is seen in residues 134–136. When the loop between $\beta$4 and $\alpha$5 is converted to conformation *B* from conformation *A*, the carboxylate group of Asp134*B*, which is in the GAA-binding site, shifts by 1.0 Å toward the substrate (Arg220′), Thr135*B* moves away from the bound SAH, losing its hydrophobic interactions with SAH, and the aromatic ring of Tyr136*B* inserts between SAH and the substrate (Arg220′) by rotating the $C_A-C_B$ bond by 135° as if it inhibits the methyl-transfer reaction. Obviously, conversion of conformation *A* to *B* is unfavorable for the catalytic reaction. Also, the presence of conformation *B* suggests that the loop between $\beta$4 and $\alpha$5 is relatively flexible in solution.

Takata and coworkers have found that Tyr136 becomes a radical under UV-light irradiation and links to the bound SAM (Takata & Fujioka, 1992). A mutagenesis study showed that a Y136F mutation results in only small changes in the

**Table 1**
Crystallographic statistics.

Values in parentheses are for the outer shell: 2.8–2.92 Å resolution for the monoclinic modification and 2.5–2.61 Å resolution for the Gd-derivative of the tetragonal modification.

| | Monoclinic modification | Gd derivative of tetragonal modification |
|---|---|---|
| Diffraction data | | |
| Unit-cell parameters (Å, °) | $a$ = 54.15, $b$ = 162.37, $c$ = 55.70, $\alpha$ = 90, $\beta$ = 96.4, $\gamma$ = 90 | $a$ = 54.22, $b$ = 54.22, $c$ = 156.27, $\alpha$ = 90, $\beta$ = 90, $\gamma$ = 90 |
| Space group | $P2_1$ | $P4_3$ |
| Resolution (Å) | 55.0–2.80 | 54.5–2.50 |
| Total observations | 122476 | 110383 |
| Unique reflections | 23416 | 14284 |
| Completeness (%) | 99.4 (88.9) | 91.2 (81.3) |
| $R_{sym}$† (%) | 6.7 (13.9) | 5.4 (9.8) |
| Refinement | | |
| No. subunits in asymmetric unit | 4 | 2 |
| Cofactors (SAH) | 4 | 2 |
| Solvent molecules ($H_2O$) | 150 | 196 |
| Resolution range (Å) | 8.0–2.8 | 8.0–2.5 |
| Total reflections used in $R_{cryst}$ | 21769 | 13620 |
| Total reflections used in $R_{free}$ | 2098 | 1341 |
| $R_{cryst}$‡ | 0.215 (0.269) | 0.194 (0.251) |
| $R_{free}$ | 0.287 (0.342) | 0.288 (0.384) |
| R.m.s.d. bond distances (Å) | 0.008 | 0.008 |
| R.m.s.d. bond angles (°) | 1.3 | 1.3 |
| R.m.s.d. torsion angles (°) | 27.7 | 27.6 |
| Residues in most favored region (%) | 87.3 | 92.8 |
| Residues in additional allowed region (%) | 12.7 | 7.2 |

† $R_{sym} = \sum |I - \langle I \rangle| / \sum |I|$. ‡ $R_{cryst} = \sum F_o - F_c| / \sum |F_o|$.

**Table 2**
Gd-coordination geometry found in the PDB files.

| Protein name and Gd-derivative and native PDB codes | Coordination No. and coordinated atoms | R.m.s.d. between the native and Gd-derivative structures (Å) (No. $C^{\alpha}$ used) | Comments |
|---|---|---|---|
| Guanidinoacetate methyltransferase (1p1c, 1khh) | 8: Glu140*A* OE1, Glu140*A* OE2, Glu141*A* OE1, Ala179*B* O, Pro106*A*′ O, $3H_2O$ | 0.26 (386) | This study |
| Inositol monophosphatase (2hhm, 1tme) | 9: Glu70 OE1, Asp90 OD1, Asp90 OD2, Ile92 O, Thr95 OG, $PO_4$ OP1, $PO_4$ OP2, $2H_2O$ | 0.36 (544) | Structure was determined by SIRAS |
| ADP-ribose pyrophosphatase (1ga7, 1gos) | 8: Glu112 OE1, Glu112 OE2, Glu115 OE1, Glu115 OE2, Glu164 OE1, Glu164 OE2, $2H_2O$ | 0.29 (403) | Structure was determined by MIR |
| Transducin $\beta\gamma$ (2trc, —) | 6+: GluP161 OE1, GluP161 OE2, GluP218 OE1, GluP218 OE2, $2H_2O$ | — | Structure was determined by MAD with Gd derivative; there is a large space to fill with one or two water molecules; two other Gd ions form a binuclear complex |
| Metabotropic glutamate receptor (1isr, —) | 6+: Asp493 OD1, Asp493 OD2, Asp493′ OD1, Asp493′ OD2, Glu386′ OE1, Glu386′ OE2 | — | Gd derivative was crystallized in a different space group; no water was included |
| Lysozyme with HPDO3A (1h87, —) | 9: N1, N2, N3, N4, O1, O3, O5, O7 from HPDO3A, $H_2O$ | — | Gd was in the cage molecule (HPDO3A); structure was determined by SIRAS |

kinetic parameters (Takata *et al.*, 1994). These studies indicate that Tyr136 is located near the bound SAM but is not involved in the catalytic reaction. However, the Y136V mutation significantly increases the values of $K_M^{SAM}$ and $K_M^{GAA}$ by 14-fold and 1100-fold, respectively, and the catalytic efficiencies ($k_{cat}/K_M$) for SAM and GAA are reduced to 2.0 and 0.026% of the wild-type enzyme values, respectively (Hamahata *et al.*, 1996). A valine residue is much smaller than a tyrosine residue and can be accommodated in the space occupied by a Tyr residue without major conformational changes in the protein

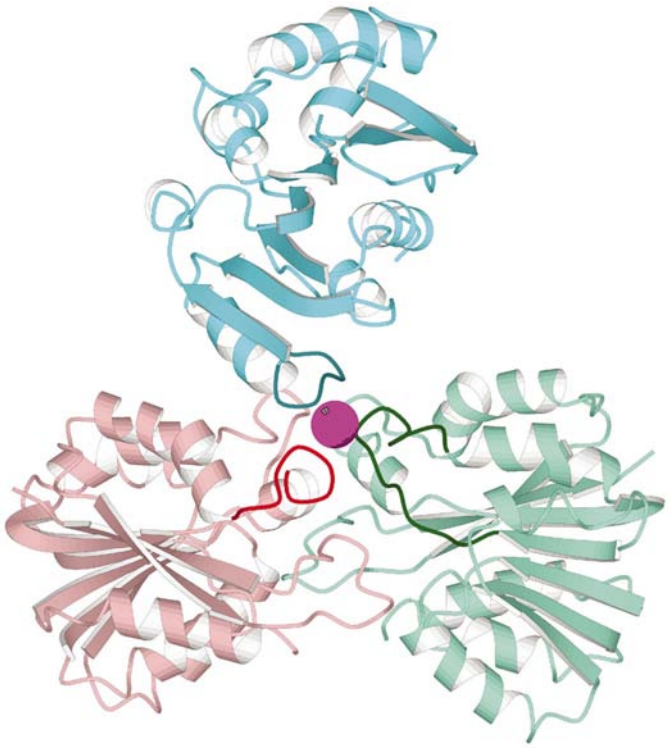

**Figure 4**
One Gd ion held by three loops from three subunits. Subunits *A*, *B* and *A*′ are colored aquamarine, light pink and cyan, respectively. The Gd ion is illustrated as a magenta ball. The three loops that hold the Gd ion are illustrated in a slightly darker color.

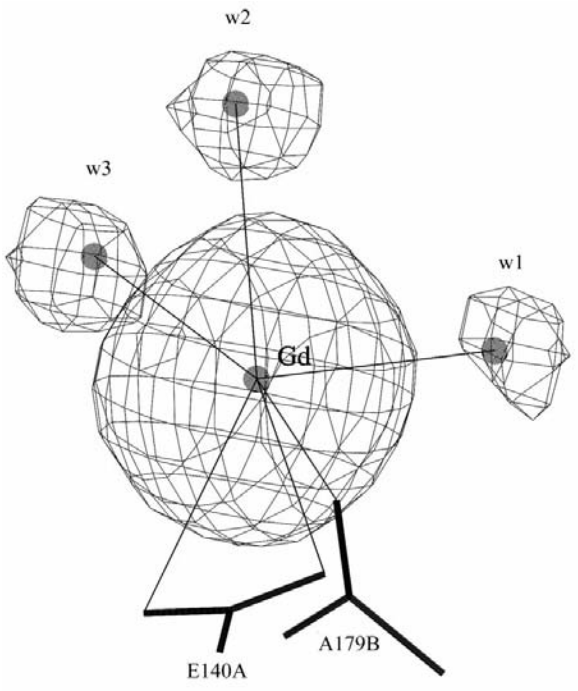


**Figure 5**
Electron-density peaks of the Gd ion and water molecules (W1, W2 and W3). The electron-density peaks of the water molecules and Gd ion were from $(F_o - F_c)$ maps calculated with the refined GAMT coordinates with and without the Gd coordinate, respectively. The contours for the Gd ion and water molecules are drawn at $3.0\sigma$ and $2.0\sigma$ levels, respectively.

structure. Thus, it was difficult to explain why the Y136V mutation causes such large increases in the $K_M$ values. As described above, the loop between $\beta$4 and $\alpha$5 has two different conformations (catalytically favorable conformation *A* and catalytically unfavorable conformation *B*). Replacement of an aromatic side chain by a small alkyl side chain at the residue 136 might shift the equilibrium of the loop conformation toward conformation *B* and thus explain why the Y136V mutated enzyme has larger $K_M$ values. The other explanation would be that the Y136V mutation changes the active-site geometry.

A preliminary X-ray study was carried out with the monoclinic crystals (Komoto *et al.*, 1999). However, we could not obtain any heavy-atom derivative crystals for MIR phasing. The GAMT structure was determined with the tetragonal crystals, using a Gd derivative for single isomorphous replacement with anomalous scattering (SIRAS). We obtained a nearly perfect isomorphous Gd-derivative crystal by a simple soaking and the Gd atom gave a significant anomalous dispersion signal with Cu $K\alpha$ radiation (Komoto *et al.*, 2002).

The crystal structure of the Gd-derivative GAMT (tetragonal modification) was refined in order to elucidate the Gd-coordination geometry. The crystallographic asymmetric unit of the tetragonal modification contains two subunits (*A* and *B*) and each subunit is related by non-crystallographic twofold symmetry. The r.m.s.d. between the native and Gd-derivative structures is 0.44 Å, indicating that Gd ions bind to GAMT molecules without significantly altering the native structure, including the Gd-binding site in the crystal. Although the crystallographic asymmetric unit of the tetragonal crystal contains two subunits, there is only one Gd ion located in each asymmetric unit. The Gd ion is in fact held by three loops from three different subunits: namely, the loop between $\beta$4 and $\alpha$5 of subunit *A*, the loop between $\alpha$6 and $\alpha$7 of subunit *B* and the loop between $\alpha$3 and $\beta$3 of subunit *A*′ (*A*′ is related to subunit *A* by the crystallographic $4_3$ symmetry operation) (Fig. 4). The carboxylate group of Glu140*A* and the carbonyl O atom of Ala179*B* coordinate the bound Gd ion (Gd···Glu140*A* OE1 = 2.6 Å, Gd···Glu140*A* OE2 = 3.1 Å, Gd···Ala179*B* O = 3.3 Å) and three water molecules coordinate the Gd ion from the opposite face (Gd···W1 = 3.3 Å, Gd···W2 = 3.3 Å, Gd···W3 = 3.4 Å; Fig. 5). In addition to these six O atoms, the two O atoms Glu141*A* OE1 and Pro106*A*′ O apparently interact with the Gd ion (Gd···Glu141*A* OE1 = 4.1 Å, Gd···Pro106*A*′ O = 4.6 Å; Fig. 6*a*). It is noted that in a small-molecule crystal structure of Na[Gd(egta)(4.5$H_2O$)], one of the Gd···O distances is reported to be 4.38 Å (Yerly *et al.*, 2002). Since the dimer *AB* has non-crystallographic twofold symmetry, a second equivalent Gd-binding site would also be present in the dimer if there were a third loop from a symmetry-related subunit available for coordination. As described above, there is no Gd in the second site, indicating that the loop of the symmetry-related subunit (*i.e.* the loop

containing the carbonyl O of Pro106) is essential for Gd binding (Fig. 6*c*).

As described above, the structure of the monoclinic modification has a pseudo-$4_3$ axis along the crystallographic *b* axis and the dimers *AB* and *CD* are related by the pseudo-$4_3$ symmetry. Therefore, a similar Gd-ion binding site could be expected in the structure. However, as shown in Fig. 6(*b*), the loop from subunit *C* (residues 105–108) moves away from the Gd-binding site so that the carbonyl O of Pro106 cannot coordinate the Gd ion. Consequently, Gd ions cannot bind the GAMT molecules in the monoclinic crystals.

Four unique crystal structures containing Gd ions were found in the PDB. Those are inositol monophosphatase (PDB code 2hhm; Bone *et al.*, 1992), transducin $\beta\gamma$ (PDB code 2trc; Gaudet *et al.*, 1996), metabotropic glutamate receptor (PDB code 1isr; Tsuchiya *et al.*, 2002) and ADP-ribose pyrophosphatase (PDB code 1ga7; Gabelli *et al.*, 2001). The Gd-coordination geometry in these protein structures is summarized in Table 2. Although there are only three cases, the r.m.s.d. between the $C^{\alpha}$ atoms of the native and Gd-derivative structures are relatively small (less than 0.36 Å), suggesting that the Gd-derivative crystals are nearly perfectly isomorphous to the native crystals. In all cases, carboxylate groups of Glu and/or Asp residues in the polypeptide chain coordinate Gd ions. The Gd-binding sites have a bowl-shaped surface constructed from at least four O atoms from the protein molecule. In addition to these O atoms, a few water molecules also coordinate the Gd ion. The results of this survey and the Gd-binding scheme seen in the GAMT structure are consistent with each other. Girard *et al.* (2002) co-crystallized hen egg-white lysozyme with a small cage compound (HPDO3A) containing Gd ion in order to examine the phasing power of the Gd ion. They reported that one Gd ion produces a strong anomalous dispersion signal with Cu *Kα* radiation to produce a high-quality SIRAS map. As described above, the dimeric GAMT structure (386 amino-acid residues) was determined with one Gd derivative using the anomalous dispersion signal from Cu *Kα* radiation. In conclusion, Gd ions can bind to proteins without changing the native protein structures, Gd atoms produce strong anomalous signals from Cu *Kα* radiation and Gd-ion binding to protein requires a relatively specific geometry.

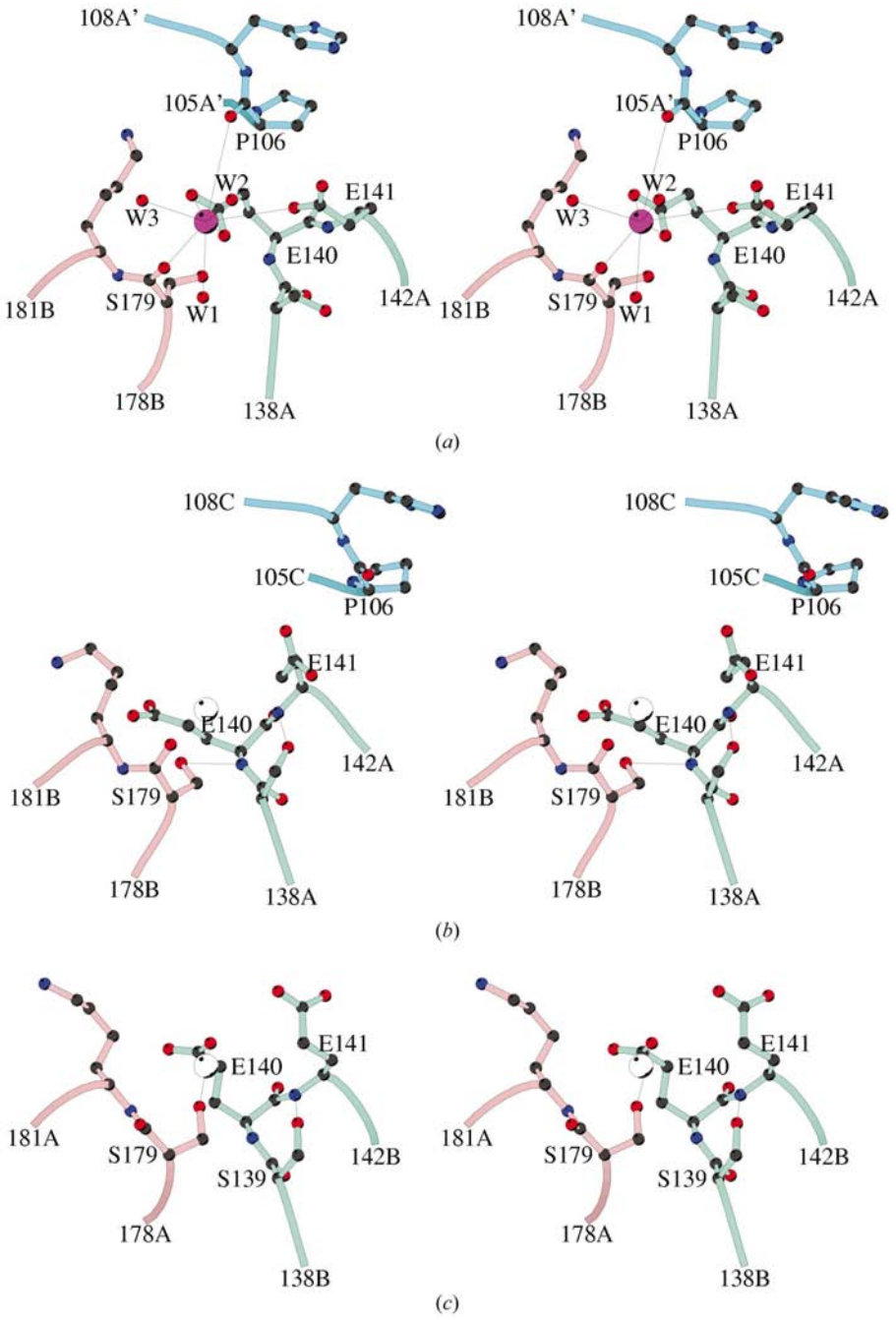


**Figure 6**
Gd-binding site and possible Gd-binding sites. (*a*) The Gd-binding site found in the tetragonal modification. Possible interactions between Gd and protein/water are illustrated by thin lines. (*b*) The equivalent site (white circle) in the monoclinic modification. (*c*) The possible Gd-binding site (white circle) related by the non-crystallographic twofold symmetry in the structure of the tetragonal modification.

This work was supported by NIH grant GM37233.

## References

Bone, R., Springer, J. P. & Atack, J. R. (1992). *Proc. Natl Acad. Sci. USA*, **89**, 10031–10035.

Brünger, A. T. (1993). *X-PLOR* v. 3.82. *A System for X-ray Crystallography and NMR*. New Haven: Yale University Press.
Cantoni, G. L. & Vignos, P. J. Jr (1954). *J. Biol. Chem.* **209**, 647–659.
Fujioka, M., Takata, Y. & Gomi, T. (1991). *Arch. Biochem. Biophys.* **285**, 181–186.
Gabelli, S. B., Bianchet, M. A., Bessman, M. J. & Amzel, L. M. (2001). *Nature Struct. Biol.* **8**, 467–472.
Gaudet, R., Bohm, A. & Sigler, P. B. (1996). *Cell*, **87**, 577–588.
Girard, E., Chantalat, L., Vicat, J. & Kahn, R. (2002). *Acta Cryst.* D**58**, 1–9.
Hamahata, A., Takata, Y., Gomi, T. & Fujioka, M. (1996). *Biochem. J.* **317**, 141–145.
Komoto, J., Huang, Y., Hu, Y., Takata, Y., Konishi, K., Ogawa, H., Gomi, T., Fujioka, M. & Takusagawa, F. (1999). *Acta Cryst.* D**55**, 1928–1929.
Komoto, J., Huang, J., Takata, Y., Yamada, T., Konishi, K., Ogawa, H., Gomi, T., Fujioka, M. & Takusagawa, F. (2002). *J. Mol. Biol.* **320**, 223–235.
Kraulis, P. J. (1991). *J. Appl. Cryst.* **24**, 946–950.
Laskowski, R. A., MacArthur, M. W., Moss, D. S. & Thornton, J. M. (1993). *J. Appl. Cryst.* **26**, 283–291.
Mudd, H. S. & Poole, J. R. (1975). *Metabolism*, **24**, 721–735.
Mudd, S. H., Ebert, M. H. & Scriver, C. R. (1980). *Metab. Clin. Exp.* **29**, 707–720.
Navaza, J. (1994). *Acta Cryst.* A**50**, 157–163.
Ogawa, H., Date, T., Gomi, T., Konishi, K., Pitot, H. C., Cantoni, G. L. & Fujioka, M. (1988). *Proc. Natl Acad. Sci. USA*, **85**, 694–698.
Otwinowski, Z. & Minor, W. (1997). *Methods Enzymol.* **276**, 307–326.
Stöckler, S., Holzbach, U., Hanefeld, F., Marquardt, I., Helms, G., Requart, M., Hänicke, W. & Frahm, J. (1994). *Pediatr. Res.* **36**, 409–413.
Stöckler, S., Isbrandt, D., Hanefeld, F., Schmidt, B. & von Figura, K. (1996). *Am. J. Hum. Genet.* **58**, 914–922.
Stöckler, S., Marescau, B., De Deyn, P. P., Trijbels, J. M. & Hanefeld, F. (1997). *Metabolism*, **46**, 1189–1193.
Takata, Y. & Fujioka, M. (1992). *Biochemistry*, **31**, 4369–4374.
Takata, Y., Konishi, K., Gomi, T. & Fujioka, M. (1994). *J. Biol. Chem.* **269**, 5537–5542.
Tsuchiya, D., Kunishima, N., Kamiya, N., Jingami, H. & Morikawa, K. (2002). *Proc. Natl Acad. Sci. USA*, **99**, 2660–2665.
Yerly, F., Hardcastle, K. I., Helm, L., Aime, S., Botta, M. & Merbach, A. E. (2002). *Chem. Eur. J.* **8**, 1031–1039.